Polythiophenes Containing In-Chain Cobaltabisdicarbollide Centers

Bruno Fabre,*,† Erhong Hao,‡ Zorabel M. LeJeune,‡ Edith K. Amuhaya,‡ Frédéric Barrière,† Jayne C. Garno,‡ and M. Graça H. Vicente*,‡

Université de Rennes 1, CNRS UMR 6226, Sciences Chimiques de Rennes, Matière Condensée et Systèmes Electroactifs (MaCSE), Campus de Beaulieu, 35042 Rennes Cedex, France, and Department of Chemistry, Louisiana State University, Baton Rouge, Louisiana 7080

ABSTRACT New cobalt(III) bis(dicarbollide) complexes covalently linked to two 2-oligothienyl units have been synthesized and electropolymerized in acetonitrile electrolyte in order to produce the corresponding polythiophene films containing in-chain metallic centers. The polymer films electrogenerated from the bithienyl (**4b**) and terthienyl (**4c**) derivatives display redox processes attributed to the Co(III)/Co(II) couple at ca. −1.1 V vs SCE and to the p-doping/undoping of the expected quaterthienyl and sexithienyl segments at ca. 0.8 V vs SCE. In contrast, the anodic oxidation of the thienyl (**4a**) derivative leads to passivation of the electrode surface. As the length of the oligothiophene substituents increases, the metallic and dicarbollide cage carbon atoms contributions in the HOMO decrease dramatically so that the highest occupied frontier orbitals of **4b** and **4c** can be considered as almost purely oligothiophene-based. From further UV−vis spectroscopy analysis, it is demonstrated that the polymer incorporating the sexithienyl segments is more conjugated than that with the quaterthienyl segments as the absorption maximum for the interband $\pi-\pi^*$ transition was observed at 410 and 448 nm for poly(**4b**) and poly(**4c**) respectively. Furthermore, these polymers display a more extended degree of conjugation than the parent oligothiophenes. Such features indicate a significant electronic delocalization through the cobaltabisdicarbollide moiety. Their conducting probe atomic force microscopy characterization indicates that poly(**4b**) and poly(**4c**) behave like heavily doped semiconductors rather than pure semiconductors. Mean conductivity values extracted from the current−voltage profiles are 1.4×10^{-4} and 7.5×10^{-4} S cm^{-1} for poly(**4b**) and poly(**4c**), respectively. Such materials are found to be efficient for the electrocatalytic reduction of protons to dihydrogen, as exemplified for poly(**4b**). The overpotential for hydrogen evolution is significantly decreased by ca. 230 mV with respect to that obtained with the bare electrode (measured for a current density of 1.4 mA cm^{-2} in the presence of 20 mM HBF_4).

KEYWORDS: conducting polymers • metallopolymers • polythiophenes • carboranes • electropolymerization

1. INTRODUCTION

Carboranes, in both neutral and anionic forms, are boron clusters with delocalized electrons and unique properties, including high hydrophobic character, low nucleophilicity, electron-withdrawing nature, and exceptional chemical, thermal, and optical stabilities as a result of their three-dimensional aromatic character (1, 2). Furthermore, complexation of the anionic open cage carborane derivatives with a variety of metal ions (e.g., Fe, Ni, and Co) leads to highly stable sandwich-type metalla-bis(dicarbollide) compounds (3, 4). Depending upon the valence of the metal these compounds can be neutral or charged, usually with one or two negative charges. These metal complexes have received much interest because of their prominent role in the extraction of radionuclides from nuclear wastes (5), in molecular recognition (6, 7), in biomedicine (8, 9), and in the construction of redox-switched molecular rotors (10, 11). For example, Hawthorne and co-workers have reported that nickel bisdicarbollide has a rotation barrier of ~6 kcal/mol and that it rotates depending on the valence of the metal, when actuated by electrical or light energy (10). Several carborane-containing organic molecules have been synthesized in the last decades and some of these are currently finding applications in medicine (12–14) and in materials science (15, 16). Furthermore, their incorporation within organic materials has been demonstrated to be valuable to confer novel properties upon the host matrix, such as high thermal and chemical stability, unique optoelectronic characteristics and an ordered structure. Several polymers containing carborane groups, usually linked to the host molecule by aromatic spacers, have been synthesized and characterized (17–22). These macromolecular systems showed extreme resistance to combustion and a two-dimensional grid-shaped structure using the boron cage as a molecular connector. However, such materials were usually synthesized in several steps and did not show peculiar electronic conducting properties, which preclude them from certain applications, such as electrochromic and charge storage devices, and electroresponsive sensors. Some years ago, Teixidor's group (23–26) and ourselves (27–31) prepared novel electroconducting polypyrroles and polythiophenes functionalized with various neutral and anionic carboranes, either via side-chain modification or direct incorporation into the polymer backbone. These materials, which were elec-

* Corresponding author. E-mail: fabre@univ-rennes1.fr (B.F.); vicente@lsu.edu (M.G.H.V.).
Received for review October 29, 2009 and accepted February 3, 2010
† Université de Rennes.
‡ Louisiana State University.
DOI: 10.1021/am9007424

Scheme 1. Synthesis of Oligothiophene-Disubstituted Cobaltabisdicarbollide Compounds

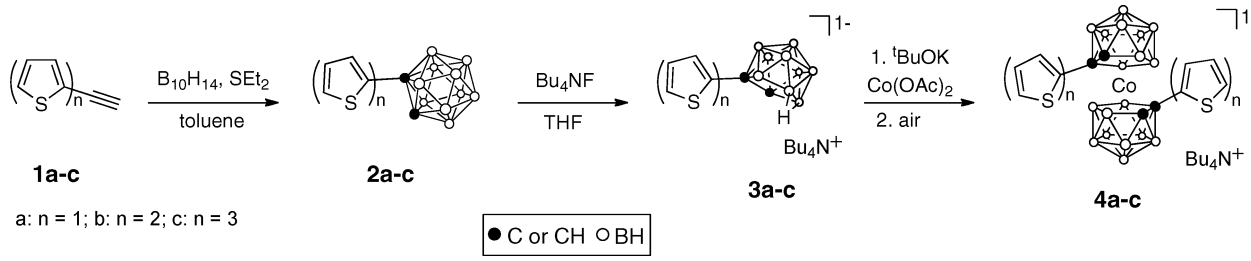

trochemically generated in one step, exhibited a strong enhancement of their electrochemical stability and overoxidation resistance compared with unsubstituted parent conducting polymers. Recently, carborane-substituted polyfluorenes were prepared which showed advantageous luminescent properties for light-emitting diodes (32, 33).

Within the attractive class of boron clusters, the metallabisdicarbollide complexes offer novel opportunities to prepare unprecedented conducting metallopolymers. Toward this goal, we report herein the synthesis and characterization of cobalt(III) bisdicarbollide derivatives covalently linked to electropolymerizable 2-oligothienyl units (Scheme 1). It was expected that oxidative coupling of the aromatic rings would lead to polythiophene films with the metal complexes incorporated in the main polymer chain. Metal-containing polymers have been the focus of intense investigations because of their potential applications in catalyses and in ion or small molecule binding (34). A central issue in the development of conducting metallopolymers is the control of the interactions between metal centers and the conducting organic polymer backbone. Compared with other conducting polymers bearing a metal center, either through a spacer arm or by electrostatic entrapment, the presence of the metal center in the conjugated chain of the polymer is expected to significantly impact on the electronic conductivity and the magnetic and optical properties of such materials. Moreover, in addition to these interesting effects, the presence of in-chain metalla-bisdicarbollide complex may also confer improved thermal and electrochemical stabilities to the host conducting material, as previously demonstrated for other carborane-functionalized polypyrroles (24, 25, 27, 29, 30) and polythiophenes (27, 28). The new conducting polymers resulting from electropolymerization of the substituted cobaltabisdicarbollides have been characterized by electrochemistry, UV−vis spectroscopy and conducting probe atomic force microscopy in order to provide significant insights on the effects of the bound cobaltabisdicarbollide moiety on the electronic properties of the resulting conducting materials. Such metallopolymers were used for the electrocatalytic reduction of H^+ and the efficiency of the electrocatalytic process was found to be highly dependent on the thickness of the metallopolymer film.

2. EXPERIMENTAL SECTION

Synthesis of Oligothiophene-Disubstituted Cobaltabisdicarbollide Compounds. General. All reactions were monitored by thin layer chromatography (TLC) using 0.25 mm silica gel plates with or without UV indicator (60F-254). The carborane clusters were detected by emerging into a solution of $PdCl_2$ in aqueous HCl (1 g $PdCl_2$ in 80 mL water and 20 mL concentrated HCl) and heated until black spot(s) was/were seen on TLC. Silica gel from Sorbent Technologies 32−63 μm was used for flash column chromatography. ^{1}H and ^{13}C NMR were obtained on either a DPX-250 or a ARX-300 Bruker spectrometer. Chemical shifts (δ) are given in ppm relative to $CDCl_3$ (7.26 ppm, ^{1}H; 77.2 ppm, ^{13}C), CD_2Cl_2 (5.32 ppm,^{1}H; 77.2 ppm, ^{13}C) or acetone-d_6 (2.05 ppm,^{1}H; 54.0 ppm, ^{13}C). MALDI-TOF mass spectra were obtained on a Bruker ProFLEX III MALDI-TOF mass spectrometer using positive mode and dithranol as the matrix. High-resolution mass spectra were obtained by using ESI-TOF with the negative mode on an Applied Biosystems QSTAR XL quadrupole time-of-flight mass spectrometer. The isotope peaks were matched with the calculated patterns; only the most abundant peaks for each compound are listed. All solvents were obtained from Fisher Scientific (HPLC grade) and used without further purification. Toluene was dried over sodium metal and distilled. Decaborane was obtained from Katchem, Inc. (Czech Republic) and all other reagents were obtained from Sigma-Aldrich and used without further purification.

Compound 2a, Thiophene-2-*o*-carborane. Diethylsulfide (4 g, 44 mmol) was added under N_2 to decaborane (2.44 g, 20 mmol) in 30 mL of dry toluene. The mixture was stirred at 40 °C for 3 h and then at 60 °C for another 2 h. A solution of commercially available 2-ethynylthiophene **1a** (2.16 g, 20 mmol) in 30 mL of dry toluene was added and the final reaction mixture was refluxed for 2 days. The reaction was cooled to room temperature and the solvent was evaporated. Methanol (50 mL) was added and the reaction mixture was stirred for 30 min. After evaporation under reduced pressure, the resulting residue was purified by silica gel chromatography, using 20% dichloromethane in hexane as the eluent. The first major fraction was collected and dried under a vacuum, giving white crystals of **2a** (2.31 g) in 53 % yield. ^{1}H NMR ($CDCl_3$, 250 MHz) δ 7.25−7.27 (1H, m, ArH), 7.20−7.21 (1H, m, ArH), 6.90−6.92 (1H, m, ArH), 3.86 (1H, s, CH), 1.50−3.50 (br, 10H, BH). ^{13}C NMR ($CDCl_3$, 63 MHz) 137.2, 130.4, 128.3, 127.7, 72.4, 63.7. ^{11}B NMR ($CDCl_3$, 128 MHz, $BF_3.OEt_2$)δ −3.3 (d, ^1J(B,H) = 146 Hz, 1B) −6.6 (d, ^1J(B,H) = 147 Hz, 1B), −10.0 to −16.0 (br m, 8B). MALDI-TOF $[M + H]^+$ 226.3. HRMS(ESI) *m/z* calcd for $C_6H_{13}B_{10}S$, 225.1739; found, 225.1746.

Compound 2b, 2,2′-Bithiophene-5-*o*-carborane. To a 100 mL reaction flask was added decaborane (0.61 g, 5 mmol), 2-ethynyldithiophene **1b** (0.57 g, 3 mmol), dry CH_3CN (4 mL), and dry toluene (16 mL). The reaction mixture was stirred under N_2 at 80 °C for 24 h. After it was cooled to room temperature, methanol (10 mL) was added to the reaction mixture and stirred for 30 min. After removal of the solvents under vacuum, the residue was purified by silica gel chromatography, using 10% dichloromethane in hexane as the eluent. The first major fraction was collected and dried under vacuum, giving a light brown solid (0.70 g) in 76 % yield. ^{1}H NMR ($CDCl_3$, 250 MHz) δ 7.27 (1H, d, J = 5.10 Hz, ArH), 7.18 (1H, d, J = 3.00 Hz, ArH), 7.09 (1H, d, J = 3.73 Hz, ArH), 7.03 (1H, t, J = 4.48 Hz, ArH), 6.94 (1H, d, J = 3.71 Hz, ArH), 3.86 (1H, s, CH), 1.50−3.50 (br,

10H, BH). ^{13}C NMR ($CDCl_3$, 63 MHz) 140.4, 136.0, 135.2, 131.1, 128.5, 126.2, 125.3, 123.8, 72.4, 63.8. ^{11}B NMR ($CDCl_3$, 128 MHz, $BF_3.OEt_2$) δ −3.4 (d, ^1J(B,H) = 145 Hz, 1B), −6.5 (d, ^1J(B,H) = 141 Hz, 1B), −10.0 to −16.0 (br m, 8B). MALDI-TOF $[M + H]^+$ 309.5. HRMS (ESI) *m/z* calcd for $C_{10}H_{15}B_{10}S_2$, 307.1630; found, 307.1623.

Compound 2c, 2,2′,5′,2″-Terthiophene-5-*o*-carborane. This compound was prepared and isolated as described above for the synthesis of **2b**, starting from **1c** (0.25 g, 0.92 mmol) and decaborane (0.20 g, 1.62 mmol). The result was a light yellow solid (0.19 g) in 53% yield. ^{1}H NMR (CD_2Cl_2, 300 MHz) δ 7.28 (1H, br s, ArH), 7.20 (1H, br s, ArH), 7.05−7.10 (4H, m, ArH), 6.95 (1H, br s, ArH), 3.88 (1H, s, CH), 1.50−3.50 (br, 10H, BH). ^{13}C NMR (CD_2Cl_2, 63 MHz) 139.9, 138.0, 136.9, 134.9, 134.5, 131.2, 128.4, 125.9, 125.5, 124.8, 124.6, 123.6, 72.5, 64.0. ^{11}B NMR ($CDCl_3$, 128 MHz, $BF_3.OEt_2$) δ −3.2 (d, ^1J(B,H) = 143 Hz, 1B), −6.4 (d, ^1J(B,H) = 148 Hz, 1B), −10.0 to −16.0 (br m, 8B). MALDI-TOF $[M + H]^+$ 391.3. HRMS(ESI) *m/z* calcd for $C_{14}H_{17}B_{10}S_3$, 390.1468; found, 390.1475.

Compound 3a, tetrabutylammonium Thiophene-2-*o*-nido-carborane. To a solution of compound **2a** (1.13 g, 5.0 mmol) in 50 mL THF was added 10 mL of *n*-Bu_4NF solution (1.0 M in THF). The reaction mixture was stirred at 60 °C for 2 h, until no starting material was visible by TLC, and then poured into 50 mL of water and extracted with ethylacetate (3 × 50 mL). The organic layers were dried over anhydrous Na_2SO_4 and concentrated under vacuum. The resulting residue was purified by passing through a pad of silica gel, using ethylacetate for elution. The title compound was obtained as a white power (2.14 g) in 94% yield. ^{1}H NMR (acetone-d_6, 250 MHz) δ 6.95−6.96 (1H, m, ArH), 6.74−6.76 (1H, m, ArH), 6.65−6.67 (1H, m, ArH), 3.37−3.39 (8H, m, CH_2), 3.35 (1H, br, CH), 1.75−1.77 (8H, m, CH_2), 1.50−3.50 (br, 9H, BH), 1.37−1.45 (8H, m, CH_2), 0.91−1.01 (12H, m, CH_3), −2.03−2.50 (1H, br, BH). ^{13}C NMR ($CDCl_3$, 100 MHz) 150.9, 126.3, 121.9, 121.5, 60.3, 59.0, 24.0, 21.0, 19.7, 13.6. ^{11}B NMR ($CDCl_3$, 128 MHz, $BF_3.OEt_2$) δ −10.0 to −16.0 (br m, 3B), −18.0 to −20.0 (br m, 3B), −24.6 (d, ^1J (B,H) = 149 Hz, 1B), −34.7(dd, ^1J (B,H) = 43.8 Hz, ^1J (B,H) = 43.7 Hz, 1B), −37.6 (d, ^1J(B,H) = 138 Hz, 1B). HRMS (ESI) $[M\text{-}NBu_4]^-$ *m/z* calcd for $C_6H_{14}B_9S$, 214.1657; found, 214.1664.

Compound 3b, Tetrabutylammonium 2,2′-Bithiophene-5-*o*-nido-carborane. This compound was prepared as described above for the preparation of **3a**, from **2b** (0.62 g, 2.0 mmol) and 4.0 mL of *n*Bu_4NF 1.0 M solution in 20 mL of THF, in 95% yield (1.02 g). ^{1}H NMR (acetone-d_6, 250 MHz) δ 7.27 (1H, dd, J = 1.11 Hz, J = 4.02 Hz, ArH), 7.08 (1H, dd, J = 1.07 Hz, J = 2.50 Hz, ArH), 6.98 (1H, dd, J =5.04 Hz, J =1.43 Hz, ArH), 6.88 (1H, d, J = 3.69 Hz, ArH), 6.58 (1H, d, J = 3.73 Hz, ArH), 3.36−3.43 (8H, m, CH_2), 2.87 (1H, br s, CH), 1.73−1.83 (8H, m, CH_2), 1.50−3.50 (br, 9H, BH), 1.35−1.46 (8H, m, CH_2), 0.91−1.00 (12H, m, CH_3), −2.51 (br, 1H, BH). ^{13}C NMR (acetone-d_6, 63 MHz) 152.1, 138.8, 133.5, 128.6, 124.3, 123.7, 123.2, 122.9, 80.5, 77.1, 59.2, 24.3, 20.3, 13.8. ^{11}B NMR ($CDCl_3$, 128 MHz, $BF_3.OEt_2$) δ −10.0 to −16.0 (br m, 3B), −18.0 to −20.0 (br m, 3B), −24.6 (d, ^1J (B,H) = 149 Hz, 1B), −34.7 (dd, ^1J (B,H) = 43.8 Hz, ^1J (B,H) = 43.7 Hz, 1B), −37.6 (d, ^1J(B,H) = 138 Hz, 1B). HRMS (ESI) $[M\text{-}NBu_4]^-$ *m/z* calcd for $C_{10}H_{16}B_9S_2$, 298.1582; found, 298.1586.

Compound 3c, Tetrabutylammonium 2,2′,5′,2″-Terthiophene-5-*o*-nido-carborane. This compound was prepared as described above for the preparation of **3a**, from **2c** (0.18 g, 0.46 mmol) and 1.0 mL of *n*Bu_4NF 1.0 M solution in 5 mL of THF, in 85% yield (0.25 g). ^{1}H NMR (acetone-d_6, 250 MHz) δ 7.43 (1H, d, J = 4.91 Hz, ArH), 7.25 (1H, d, J = 3.41 Hz, ArH), 7.16 (1H, d, J = 3.71 Hz, ArH), 7.05−7.08 (2H, m, ArH), 6.95 (1H, d, J = 3.61 Hz, ArH), 6.59 (1H, d, J = 3.64 Hz, ArH), 3.40−3.47 (8H, m, CH_2), 3.02 (1H, br s, CH), 1.75−1.8 (8H, m, CH_2), 1.50−3.50 (br, 9H, BH), 1.36−1.44 (8H, m, CH_2), 0.93−0.99 (12H, m, CH_3), −2.40 (br, 1H, BH). ^{13}C NMR (acetone-d_6, 63 MHz) 152.1, 137.2, 137.1, 135.2, 132.6, 128.6, 125.3, 124.9, 124.1, 123.7, 123.6, 122.8, 80.8, 67.7, 59.0, 24.2, 20.0, 13.6. ^{11}B NMR ($CDCl_3$,128 MHz, $BF_3.OEt_2$) δ −10.0 to −16.0 (br m, 3B), −18.0 to −20.0 (br m, 3B), −24.6 (d, ^1J (B,H) = 149 Hz, 1B), −34.7 (dd, ^1J (B,H) = 43.8 Hz, ^1J (B,H) = 43.7 Hz, 1B), −37.6 (d, ^1J(B,H) = 138 Hz, 1B). HRMS (ESI) $[M\text{-}NBu_4]^-$ *m/z* calcd for $C_{14}H_{18}B_9S_3$, 380.1462; found, 380.1466.

Compound 4a, Tetrabutylammonium Cobalt(III) Bis-(thiophene-2-*o*-nido-carborane). Compound **3a** (458 mg, 1 mmol), *t*BuOK (1.12 g, 10 mmol), and anhydrous $CoCl_2$ (1.35 g, 10 mmol) were mixed in a 50 mL Schlenk reaction tube and 10 mL of anhydrous dimethoxyethane (DME) was added via syringe. The reaction was refluxed for 30 h under nitrogen, and then cooled to room temperature and filtered to remove the inorganic salt. The filtrate was partitioned between dichloromethane and *n*-Bu_4NHSO_4 aqueous solution, dried under a vacuum, and purified by silica gel chromatography using dichloromethane as the eluent. The first major fraction was collected and dried under a vacuum, giving a yellow powder (251 mg) in 70 % yield. ^{1}H NMR (acetone-d_6, 250 MHz) δ 7.22−7.24 (1H, m, ArH), 7.13−7.15 (1H, m, ArH), 6.89−6.91 (2H, m, ArH), 6.75−6.78 (1H, m, ArH), 6.63−6.64 (1H, m, ArH), 4.27 (1H, s, CH), 3.41−3.47 (8H, m, CH_2), 3.22 (1H, s, CH), 1.76−1.78 (8H, m, CH_2), 1.50−3.50 (18H, br, BH), 1.37−1.51 (8H, m, CH_2), 0.95−1.01 (12H, m, CH_3). ^{13}C NMR ($CDCl_3$, 100 MHz) 125.7, 125.8, 123.2, 59.1, 30.9, 24.1, 19.7, 13.7. ^{11}B NMR ($CDCl_3$, 128 MHz, $BF_3.OEt_2$) δ 9.0−30.0 (br m, max at 5.9, −0.5, −8.8 and −30.8, 18B) ppm. HRMS (ESI) $[M\text{-}NBu_4]^-$ *m/z* calcd for $C_{12}H_{26}B_{18}S_2Co$, 488.26; found, 488.2628.

Compound 4b, Tetrabutylammonium Cobalt(III) Bis(2,2′-bithiophene-5-*o*-nido-carborane). This compound was prepared as described above for the synthesis of **4a**, from **3b** (541 mg, 1 mmol), *t*BuOK (1.12 g, 10 mmol), and anhydrous $CoCl_2$ (1.35 g, 10 mmol), and was obtained (0.28 g) in 63% yield as a dark yellow solid. ^{1}H NMR (acetone-d_6, 250 MHz) δ 7.19−7.28 (3H, m, ArH), 7.06−7.09 (2H, m, ArH), 6.98−7.04 (2H, m, ArH), 6.79 (2H, br s, ArH), 6.41 (1H, br s, ArH), 4.17 (1H, br s, CH), 3.32 (1H, br s, CH), 3.07−3.11 (8H, m, CH_2), 1.60−1.62 (8H, m, CH_2), 1.50−3.50 (18H, br, BH), 1.37−1.46 (8H, m, CH_2), 1.00−1.06 (12H, m, CH_3). ^{13}C NMR ($CDCl_3$, 100 MHz) 127.6, 127.4, 124.7, 123.5, 123.2, 122.8, 59.2, 43.0, 24.0, 19.8, 13.7. ^{11}B NMR ($CDCl_3$, 128 MHz, $BF_3.OEt_2$) δ 9.0−30.0 (br m, max at 5.9, −0.5, −8.8 and −30.8, 18B) ppm. HRMS (ESI) $[M\text{-}NBu_4]^-$ *m/z* calcd for $C_{20}H_{30}B_{18}S_4Co$, 652.2346; found, 652.2362.

Compound 4c, Tetrabutylammonium Cobalt(III) Bis-(2,2′,5′,2″-terthiophene-5-*o*-nido-carborane). This compound was prepared as described above for the synthesis of **4a**, from **3c** (0.22 mg, 0.35 mmol), *t*BuOK (0.23 g, 2 mmol), and anhydrous $CoCl_2$ (0.27 g, 2 mmol), and was obtained (0.108 g) in 61% yield as a dark yellow solid. ^{1}H NMR (acetone-d_6, 250 MHz) δ 7.40−7.43 (2H, m. ArH), 7.25−7.27 (2H, m, ArH), 7.16−7.18 (2H, m, ArH), 7.05−7.08 (4H, m, ArH), 6.81−6.97 (2H, m, ArH), 6.50−6.61 (2H, m, ArH), 3.60 (1H, br s, CH), 3.40−3.47 (8H, m, CH_2), 3.10 (1H, br s, CH), 1.73−1.81 (8H, m, CH_2), 1.50−3.50 (18H, br, BH), 1.37−1.45 (8H, m, CH_2), 0.95−1.00 (12H, m, CH_3). ^{13}C-NMR ($CDCl_3$, 100 MHz) 138.1, 137.9, 135.1, 132.5, 127.5, 126.2, 124.8, 123.9, 123.5, 122.7, 68.7, 58.9, 42.6, 24.2, 20.0, 13.6. ^{11}B NMR ($CDCl_3$, 128 MHz, $BF_3.OEt_2$) δ 9.0−30.0 (br m, max at 5.9, −0.5, −8.8 and −30.8, 18B) ppm. HRMS (ESI) $[M\text{-}NBu_4]^-$ *m/z* calcd for $C_{28}H_{34}B_{18}S_6Co$, 816.2129; found, 816.2115.

Electrochemical Characterizations. Linear potential sweep cyclic voltammetry experiments were performed with an Autolab PGSTAT 20 potentiostat from Eco Chemie B.V., equipped with General Purpose Electrochemical System GPES software (version 4.5 for Windows). The working electrode was a 1 mm diameter platinum or glassy carbon disk (area: 8×10^{-3} cm^2) and the counter electrode was a glassy carbon rod. Potentials

were relative to the system 1×10^{-2} M Ag^+ | Ag in acetonitrile used as the reference electrode (+0.29 V vs aqueous SCE). All reported potentials are referred to SCE (± 0.01 V). Tetra-*n*-butylammonium hexafluorophosphate Bu_4NPF_6 was purchased from Fluka (puriss, electrochemical grade) and was used at 0.1 mol L^{-1} as supporting electrolyte in acetonitrile (anhydrous, analytical grade from SDS). The (CH_3CN + 0.1 M Bu_4NPF_6) electrolytic medium was dried over activated, neutral alumina (Merck) for 30 min, under stirring, and under argon. Alumina was previously activated at 450 °C under a vacuum for several hours. About 7 mL of this solution was transferred with a syringe into the electrochemical cell prior to experiments. All electrochemical measurements were carried out inside a homemade Faraday cage at room temperature (20 ± 2°C) and under a constant flow of argon.

UV−Visible Spectroelectrochemistry. UV−visible absorption spectra were recorded on a Shimadzu Multispec-1501 spectrophotometer (190−1100 nm scan range) interfaced with a microcomputer for data acquisition and using quartz SUPRASIL cells from Hellma (1 cm pathlength). The polymer films were grown on an indium tin oxide (ITO)-coated glass slide electrode.

Computational Details. Geometry optimizations of **4a−c** models in a cisoid conformation were carried out with density functional theory (DFT) (35, 36) calculations and performed with the hybrid Becke three-parameter exchange functional (37 −39) and the Lee−Yang−Parr nonlocal correlation functional (40) (B3LYP) implemented in the Gaussian 03 (Revision D.02) program suite (41) using the LanL2DZ basis set (42–44) and the default convergence criteria implemented in the program. The figures were generated with MOLEKEL 4.3 (45).

Conducting Probe Atomic Force Microscopy (AFM). Samples of doped and undoped cobaltabisdicarbollide-functionalized polythiophene films were prepared on gold surfaces on glass (EMF Corporation, Ithaca, NY) using controlled potential electropolymerization. The electropolymerization potentials were previously optimized using cyclic voltammetry experiments with millimetric platinum electrodes. The substrates have a gold coating (1000 Å) on a 50 Å layer of Cr formed on glass. Surface characterizations were accomplished in ambient conditions using a model 5500 scanning probe microscope (SPM) equipped with Picoscan v5.3.3 software (Agilent Technologies, Inc., Chandler, AZ). Characterizations of the surface morphology were accomplished using intermittent or tapping mode atomic force microscopy (AFM). Tapping mode AFM images were acquired at a scan rate of 3.0 nm s^{-1} rastered for 512 lines per frame. Monolithic silicon probes (PPP-NCL) from Nanosensors (Neuchâtel, Switzerland**)** were used for tapping mode experiments, with an average force constant of 48 N m^{-1} and resonant frequency of 172 kHz. A multipurpose SPM scanner with a scanning area of 11 × 11 μm^2 was used for imaging, with interchangeable nose cones for either tapping mode or conductive probe AFM experiments. For tapping-mode, the nose cone contains a small piezoceramic chip for tip actuation. For current imaging and *I*−*V* measurements, a preamp is integrated within the nose cone. Conductive probe AFM experiments were accomplished using a V-shaped conductive AFM tip (CSC11/Ti-Pt, Micromasch, San Jose, CA) coated with 10 nm Pt layer on a sublayer of 20 nm Ti. All AFM images were processed with free and open source software for data visualization and analysis, Gwyddion (version 2.5) supported by the Czech Metrology Institute (http://gwyddion.net/). Gwyddion is a modular program for SPM data visualization and analysis. Estimates of surface coverage were obtained with UTHSCA Image Tool (46). The AFM current images were converted to grayscale bitmaps and a threshold value was selected visually for conversion to black and white pixels. The percentage of colored pixels provided a relative estimate of surface coverage.

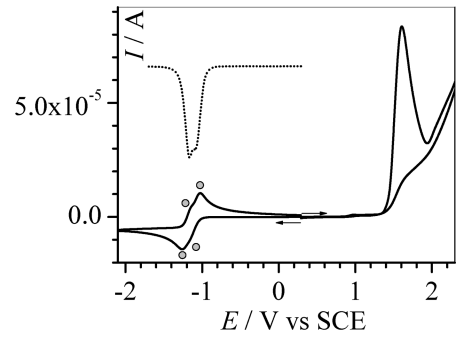

FIGURE 1. Cyclic (solid line) and differential pulse (dotted line) voltammograms of 4a at 1×10^{-2} M in CH_3CN + 10^{-1} M Bu_4NPF_6 (0.1 V s^{-1}).

Table 1. Cyclic Voltammetry Data of Oligothienylcobaltabisdicarbollide Complexes at 1×10^{-2} M (except for 4c, 5×10^{-3} M) in CH_3CN + 10^{-1} M Bu_4NPF_6; Potential Scan Rate = 0.1 V s^{-1}

compd	reduction $E^{\circ\prime}$ (V vs SCE)[a]	oxidation E_{pa} (V vs SCE)[b]
4a	−1.06 (78); −1.19 (83)	1.60_5
4b	−1.03 (60); −1.12 (60)	1.21 (sh); 1.37; 1.58 (sh); 1.85 (sh); 2.18
4c	−1.07 (114)	0.88; 0.98; 1.24; 1.49; 1.75 (sh)

[a] Average of anodic and cathodic peak potentials; the peak-to-peak separation in mV is indicated between brackets. [b] Irreversible processes; sh = shoulder.

3. RESULTS AND DISCUSSION

3.1. Synthesis of Oligothiophene-Disubstituted Cobaltabisdicarbollide Compounds. As shown in Scheme 1, compounds **2a−c** were synthesized in 53−76% yield from decaborane, ethyl sulfide and the terminal thienylacetylenes **1a−c** (47, 48). Deboronation of the ortho-carborane cages of **2a−c** using *n*Bu_4NF (49) gave the corresponding nido-carborane derivatives **3a−c** as the *n*Bu_4N^+ salts, in almost quantitative yields. The cobalt(III) complexes **4a−c** were synthesized in a two-step/one-pot procedure, by mixing *t*BuOK and $Co(OAc)_2$ in dimethoxyethane (50), followed by air oxidation in 61−70% overall yields. The target complexes **4a−c** were characterized by NMR and HRMS, which gave the expected isotope pattern distributions (see the Supporting Information).

3.2. Electrochemical Characterization of Oligo thiophene-Disubstituted Cobaltabisdicarbollides and Corresponding Conducting Polymer Films. Within the investigated potential range −2.0/2.3 V vs SCE, all compounds show redox activity in CH_3CN medium both due to the reversible reduction of Co(III) to Co(II) and to the oxidation of the thiophene rings (Figure 1 and Table 1). This assignment is consistent with the results of DFT calculations (Figure 2) that show a significant metal character in the LUMOs and a major oligothiophene character in the HOMOs of **4a−c**. First, the reversible one-electron reduction of Co(III) to Co(II) occurs between −1.2 and −1.0 V vs SCE for the three complexes and unexpectedly gives rise to two closely

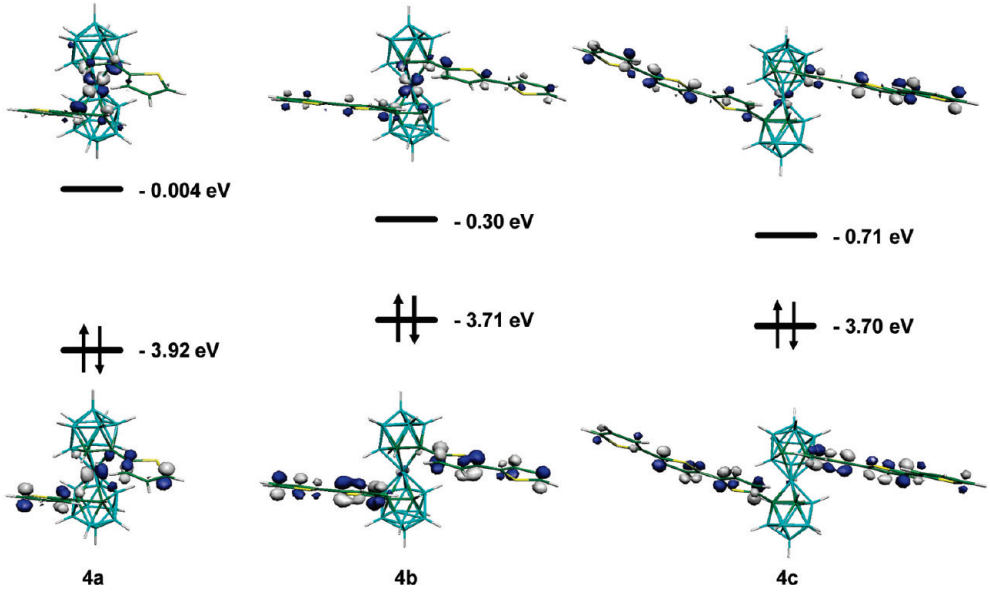

FIGURE 2. HOMOs and LUMOs of 4a−c from DFT calculations.

spaced systems for **4a** and **4b** and a single broad system for **4c**. The values of the formal potential $E^{\circ\prime}$ corresponding to each system are listed in Table 1 and the cyclic voltammogram of **4a** is shown in Figure 1 as a representative example. The separation between the two formal potentials $\Delta E^{\circ\prime}$ is found to decrease with increasing the number of thiophene rings linked to the cobaltabisdicarbollide moiety. It is obvious that the second system can not be assigned to the reduction of Co(II) to Co(I), as this process is observed at much more negative potentials, below −2.0 V vs SCE. Moreover, the Co(III)/Co(II) process of the unsubstituted cobaltabisdicarbollide is characterized by a single reversible wave at $E^{\circ\prime} = -1.34$ V vs SCE (8, 51). In the case of our study, the presence of two closely spaced systems is directly connected to the presence of the 2-oligothienyl substituents. Based on our electrochemical data, it can be proposed that the reduction of oligothienylcobaltabisdicarbollide complexes involves two redox conformers, both the relative stability and the proportion of which are strongly dependent on the number of bound thiophene rings (Scheme 2). Indeed, from Scheme 2, the parameter $\Delta E^{\circ\prime}$ can be written as a function of the equilibrium constants (eq 1).

$$\Delta E^{\circ\prime} = \frac{2.3RT}{F}\log\left(\frac{K_{\mathrm{Co(II)}}}{K_{\mathrm{Co(III)}}}\right) \qquad (1)$$

Although rotational conformers of nickel- (10, 11, 52) and cobalt-bis(dicarbollide)complexes (53) have been demonstrated by Hawthorne and Teixidor et al. respectively, electrochemical evidence of such systems has not been reported so far, to the best of our knowledge. Further investigations are required in order to define the structure of the redox conformers involved in the reduction of these oligothienylcobaltabisdicarbollide complexes. The LUMOs of **4a**−**c** have an antibonding character between the d_{xz} or d_{yz}-type metal atomic orbital and the pπ-type orbitals of the carbon atoms in the two dicarbollide cages. Populating this orbital may then trigger the relative rotation of the cages around the metal towards a more stable redox conformer. In addition, as the length of the oligothiophene substituents increases in **4a**−**c**, the calculated nature of the LUMO becomes less centered on the metallabisdicarbollide and more delocalized on the oligothiophene substituents. We note that this correlates well with the observed decrease in $\Delta E^{\circ\prime}$ values in **4a**−**c**, Table 1.

Scheme 2. Square Scheme Depicting the Different Species Involved in the Reduction of Oligothienylcobaltabisdicarbollide Complexes[a]

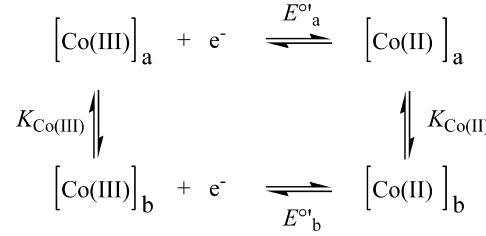

[a] $E^{\circ\prime}_a$ and $E^{\circ\prime}_b$ are the formal potentials corresponding to the Co(III)/Co(II) couple of the two conformers denoted "a" and "b", respectively. $K_{\mathrm{Co(III)}}$ and $K_{\mathrm{Co(II)}}$ are the related equilibrium constants between the two conformers for the Co(III) and Co(II) forms.

Now, oxidation of these compounds is characterized by a single irreversible peak at ca. 1.6 V vs SCE for **4a** (Figure 1) and multiple irreversible peaks in the range 1.2−2.2 V and 0.9−1.75 V for **4b** and **4c** respectively (Figure 3A,B). The irreversible nature of anodic electron transfer steps at all investigated potential scan rates (0.02−1 V s^{-1}) is consistent with the multielectronic oxidation of the 2-oligothienyl rings into reactive radical cation species. Furthermore, the oxidation potentials of these systems are found to decrease in the order **4a** > **4b** > **4c**, in agreement with the lengthening of the linked π-conjugated segment and with the result of DFT calculations (Table 1 and Figure 2). The

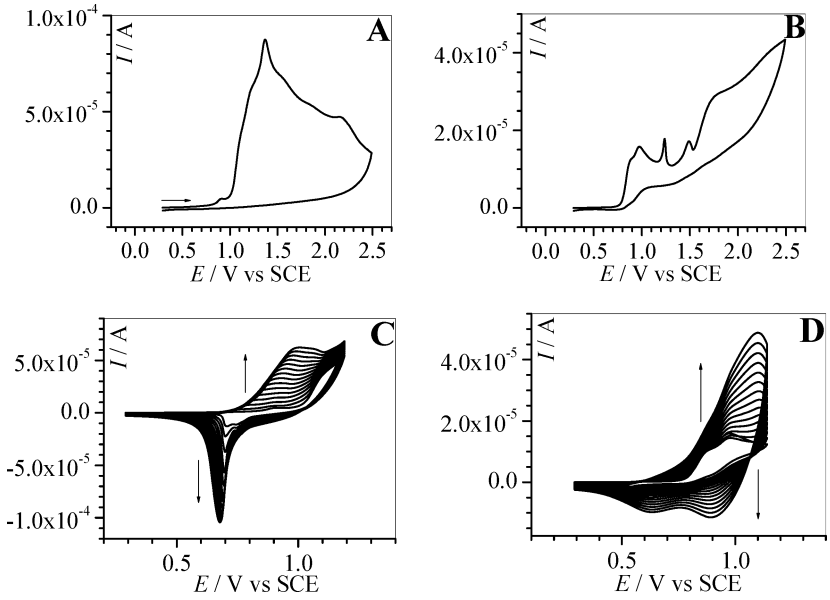

FIGURE 3. Oxidative cyclic voltammograms of (A) 4b at 1×10^{-2} M and (B) 4c at 5×10^{-3} M in $CH_3CN + 0.1$ M Bu_4NPF_6. Potentiodynamical growth of (C) poly(4b) and (D) poly(4c). Potential scan rate: 0.1 V s^{-1}.

electrochemical oxidation of **4b** and **4c** leads to the formation of conducting polymer deposits on the electrode surface. Such films could be electrogenerated either potentiodynamically or potentiostatically with no significant effect of the electropolymerization method on their respective electrochemical responses. Representative cyclic voltammograms corresponding to the potentiodynamical electropolymerization of **4b** and **4c** are shown in Figure 3C,D. These are characterized by the regular growth of a new system at less positive potentials. In contrast to the facile electropolymerization of **4b** and **4c**, **4a** does not yield a conducting polymer deposit regardless of the tested experimental conditions (by changing the monomer concentration, the oxidation potential or the solvent). Instead, a poorly electroactive film is electrogenerated, yielding the gradual passivation of the electrode surface. Such a situation has already been encountered in the case of the anodic electrochemistry of other redox-active metallic systems incorporating 2-thienyl units (54, 55) and can be explained by the high reactivity of the thiophene radical cation in close proximity of the cobaltabisdicarbollide unit which undergoes a rapid decomposition. DFT calculations indicate that the HOMO of **4a** has a mixed and balanced character between a typical organic thiophene contribution, consistent with a possible electropolymerisation, and a bonding contribution between a d_{xz} or d_{yz}-type metal atomic orbital and the pπ-type orbitals of the carbon atoms in the two dicarbollide cages (Figure 2).

Removing an electron from such an orbital may explain the decomposition of the cobaltabisdicarbollide bridges in the resulting polymer deposit. Hence, the theoretical data are consistent with the experimental passivation of the electrode with an insulating material after anodic oxidation of **4a**. As the length of the oligothiophene substituents increases, in **4b** and **4c**, the metallic and dicarbollide cage carbon atoms contributions in the HOMO decrease dramatically so that the highest occupied frontier orbitals of **4b** and **4c** can be considered as almost purely oligothiophene-based. This corroborates the observed electropolymerisation of these oligothiophenes and the stability (through the robustness of the cobaltabisdicarbollide bridges) and conductivity of the resulting polymers based on **4b** and **4c**.

Following their electrosynthesis, the electroactive poly(**4b**) and poly(**4c**) films are examined in a monomer-free electrolytic medium. First, the electrochemical response of poly(**4b**) in oxidation is characterized by a broad reversible system at $E^{\circ\prime} = 0.80-0.85$ V vs SCE corresponding to the p-doping/undoping of the expected quaterthienyl segments (Figure 4). The oxidation of sexithienyl segments in poly(**4c**) is characterized by two quasi-reversible redox processes at 0.72 and 1.00 V vs SCE (Figure 5). To evaluate the mechanism that controls the charge transport in poly(**4b**) and poly(**4c**), the anodic peak current intensities I_{pa} corresponding to the p-doping process were plotted as a function of the potential scan rate, v, in a logarithmic form. Representative plots are shown in Figure 4D for poly(**4b**) but quite similar plots are also obtained for poly(**4c**). The values of the slope for thin films are ca. 1.0, as expected for surface-immobilized electroactive species (56). A decrease in the slope from 1.0 to ca. 0.8 is observed upon increasing the film thickness. Ideally, a slope of 0.5 is obtained for semi-infinite diffusion-controlled process. These results indicate that for thick films the charge transport mechanism in poly(**4b**) and poly(**4c**) becomes controlled by the diffusion of electrolyte counterions across the polymer film to ensure the electroneutrality of the material. The doping level δ (57) of poly(**4b**) and poly(**4c**) is estimated respectively at 0.30−0.35 and 0.20−0.25 positive charge per monomer (i.e., quaterthienyl and sexithienyl respectively) unit and is somewhat independent on the film thickness. Compared with unsubstituted polythiophene, the oxidation level of both polymers is much lower, which demonstrates the prominent role of the incorporated cobaltabisdicarbollide center on the ion transport in these films. On the basis of these values of δ, the oxidation/reduction of such polymers is expected to

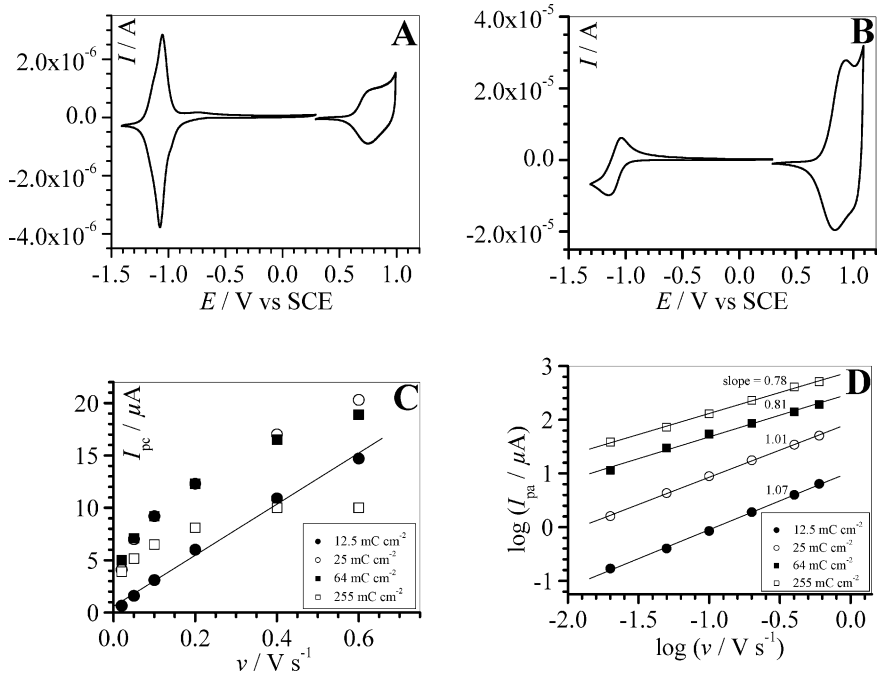

FIGURE 4. Electrochemical response of the electrogenerated poly(4b) in CH_3CN + 0.1 M Bu_4NPF_6 at 0.1 V s^{-1}. The consumed electropolymerization charge is 12.5 (A) and 64 mC cm^{-2} (B). (C) Corresponding I_{pc} vs v plots for the Co(III)/Co(II) process as a function of the film electropolymerization charge. (D) Corresponding logI_{pa} vs log$v$ for the p-doping/undoping process of poly(4b) as a function of the film electropolymerization charge.

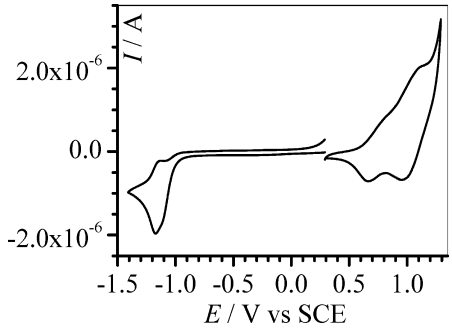

FIGURE 5. Electrochemical response of the electrogenerated poly(4c) in CH_3CN + 0.1 M Bu_4NPF_6 at 0.1 V s^{-1}. The consumed electropolymerization charge is 25 mC cm^{-2}.

involve the transport of electrolyte cations (in our case, Bu_4N^+) to neutralize the negative charge of the metallic center, as opposed to the transport of counteranions as commonly observed for the doping of polythiophenes.

Now, we shall turn towards the electrochemical behavior of these polymers when the potential is scanned towards negative potentials. As shown in Figure 4A for poly(**4b**), a perfectly reversible system is observed in reduction at −1.08 V corresponding to the Co(III)/Co(II) couple. For thin films, the peak-to-peak separation and the full width at half-maximum (fwhm) measured at low scan rates (typically 0.05 V s^{-1}) are less than 20 mV and ca. 130 mV, respectively. These values are very close to the theoretically predicted values as a zero peak-to-peak separation and a fwhm of 90 mV are expected for a surface-confined monoelectronic redox center (56). Consistent with that, the peak currents are found to vary linearly with the potential scan rate v (Figure 4C). Interestingly, upon increasing the film thickness, the system assigned to Co(III)/Co(II) becomes less and less visible and the variation of the electrochemical parameters are all consistent with a decrease in the electron-transfer rate. Indeed, the peak-to-peak separation and the fwhm increase to 130 and >270 mV respectively, and a deviation from linearity is observed in the peak currents vs v plots. Similar effects of the film thickness on the Co(III)/Co(II) response are obtained for poly(**4c**). Nevertheless, even in thin films, the Co(III)/Co(II) system is much less reversible than that observed for poly(**4b**). Indeed, the cathodic step ascribed to the Co(III) reduction is more intense than its related anodic component (Figure 5). Such intriguing effects of the film thickness on the electroactivity of the surface-confined Co(III)/Co(II) couple have already been reported by others with cobalt salen-based polymers (58, 59).

It must be kept in mind that the cobalt-centered redox process occurs within a potential range where the oligothienyl units are in their neutral reduced state, i.e., in their electronically insulating state. Consequently, the reduction of Co(III) to Co(II) is expected to occur by electron hopping between cobalt centers down to the electrode surface and involves cation migration through the film in order to ensure the electroneutrality of the material.

For thick films, a large amount of cobalt centers within the film are not electrochemically addressable because electrolyte cations can not migrate up to them. Such mass transport constraints can be explained by the more compact and less rough structure of the reduced polymer compared with the polymer in its oxidized state, as evidenced by their AFM analysis (vide infra).

3.3. UV−Visible Spectroscopy Analysis of Polymers. To gain further insight into the electronic properties of cobaltabisdicarbollide-substituted poly-

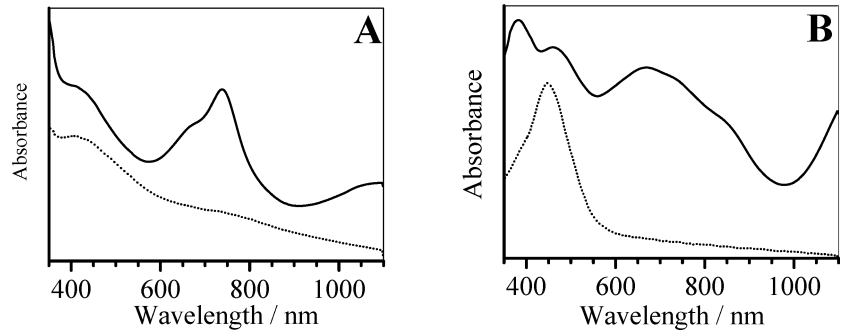

FIGURE 6. Solid-state UV−vis spectra of (A) poly(4b) and (B) poly(4c) in their doped (solid line) and reduced (dotted line) states.

thiophenes, a UV-vis spectroscopic analysis was performed focusing on the electroactive polymers electrogenerated from **4b** and **4c**. First, the UV-vis spectrum of compounds **4a**−**c** in CH_2Cl_2 consists of four absorption bands within 230−500 nm (see the Supporting Information). The two bands at 260−280 nm and 460−500 nm can be ascribed to the cobaltabisdicarbollide center (3, 60, 61), the second less intense one being due to the d−d transition in the Co metal. The bands observed at 250, 325, and 373 nm in the spectra of **4a**, **4b**, and **4c** respectively are assigned to the $\pi-\pi^*$ transition in the aromatic substituents. However, compared with the unsubstituted parent oligothiophenes (62), these bands are red-shifted by ca. 15−25 nm in the metallic complexes. Such features indicate a weak electronic delocalization through the cobaltabisdicarbollide center. The electroactive polymers in their neutral form show an absorption maximum for the interband $\pi-\pi^*$ transition at 410 and 448 nm for poly(**4b**) and poly(**4c**), respectively (Figure 6). Expectedly, the polymer incorporating the sexithiophene segments is more conjugated than that with the quaterthiophene segments. Furthermore, poly(**4b**) and poly(**4c**) display a more extended degree of conjugation than the parent oligothiophenes as quaterthiophene and sexithiophene show an absorption maximum at 388 (63) and 432 nm (64, 65), respectively. The magnitude of the red-shift is similar to that observed with the monomers (ca. 20 nm), which accounts for the same electronic influence of the cobaltabisdicarbollide on the conjugated aromatic chain of the polymer. It must be stressed that the presence of the cobaltabisdicarbollide center in the polymer films can not be evidenced from their optical spectra essentially because of the strong absorbance below 350 nm of the used optically transparent electrode and the very weak intensity of the band at 460−500 nm attributed to the cobalt complex. The as-grown oxidatively doped poly(**4b**) and poly(**4c**) films display several new doping-induced bands with maxima at 425, 664, and 738 nm for poly(**4b**) and 465, 669, 739, and 852 nm for poly(**4c**) (Figure 6). A further broad band attributed to the formation of the so-called "free carrier tail" (66) is also visible in the near IR region above 1100 nm. Similarly to the neutral forms, the bands of p-doped poly(**4b**) and poly(**4c**) are red-shifted to approximately the same extent with respect to those of oxidized quaterthienyl and sexithienyl moieties (63). The position of these doping-induced bands and the lowly doped character of the as-grown polymers indicate the formation of polaronic charge states along the polymer chain.

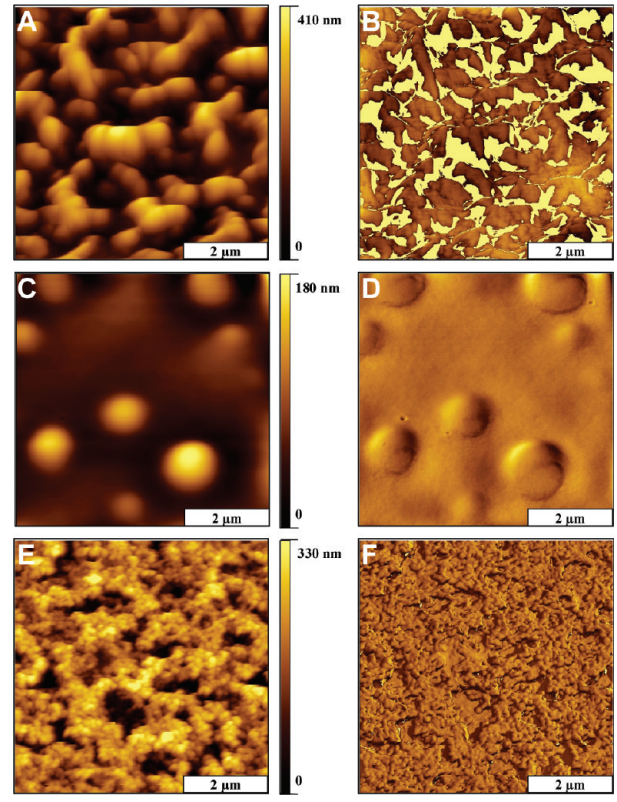

FIGURE 7. (A, C, E) Tapping-mode AFM topographs and (B, D, F) corresponding phase topographs of (A, B) neutral undoped poly(4a), (C, D) poly(4b), and (E, F) poly(4c). The scan size for all topographs is 5 × 5 μm^2.

3.4. Conducting Probe AFM Characterization of the Cobaltabisdicarbollide-Functionalized Polymers. *Nanoscale Comparison of Surface Morphologies.*

Samples of electropolymerized poly(**4a**−**c**) films in their doped and undoped forms were characterized using tapping-mode AFM in an ambient environment. Substantial differences are apparent for views of the surface morphology of the polymer films, as presented in Figures 7 and 8. The surface structures of electropolymerized films and subsequently undoped by electrochemical reduction are shown in Figure 7. Undoped poly(**4a**) exhibits irregular island domains with angular features having lateral dimensions ranging from 0.45 to 2.8 μm. The height of the domains ranges from 100 to 390 nm. The angular domains cover 66% of the surface and the root-mean-square (rms) surface

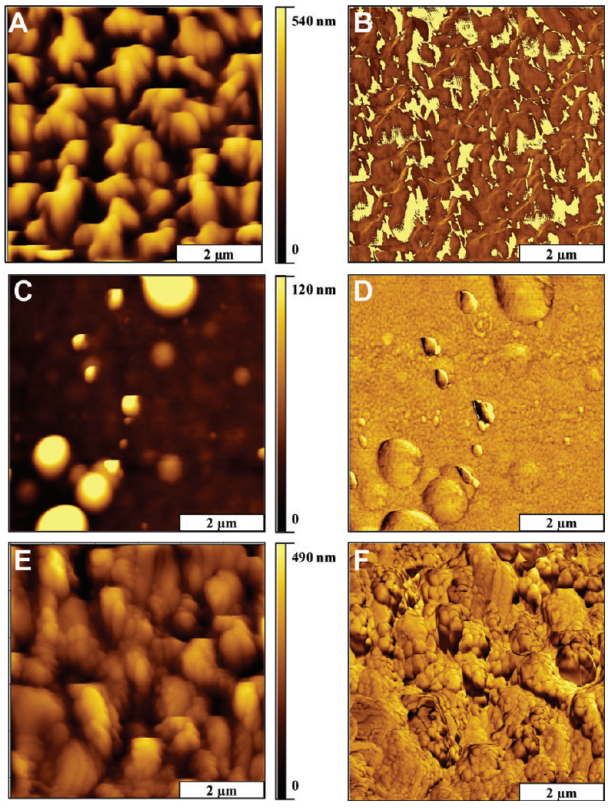

FIGURE 8. (A, C, E) Tapping-mode AFM topographs and (B, D, F) corresponding phase topographs of as-grown *p*-doped (A, B) poly(4a), (C, D) poly(4b), and (E, F) poly(4c). The scan size for all topographs is 5 × 5 μm^2.

roughness is estimated at 81 nm. A closer view (5 × 5 μm^2) reveals that the larger domains are made of segments that are tightly packed to form larger assemblies (Figure 7A). Interesting features are observed in the corresponding phase image (Figure 7B), in which the groove areas are displayed with a bright yellow color due to saturation. Although results for distinguishing differences in surface chemistry are not conclusive, the phase image is still useful for identifying edges of surface features. The surface of the undoped poly(**4b**) exhibits isolated globular structures of different sizes (Figure 7C). The smooth round domains range from 0.5 to 2.0 μm in lateral dimension and the heights range from 23 to 180 nm. The smooth globular domains cover 23% of the surface and the local surface roughness measures 19 nm. The simultaneously acquired phase image (Figure 7D) displays a relatively homogeneous color for the globular domains and flatter areas of the film, which indicates a uniform surface composition for the film. The faint dark shadows which outline the round features can be attributed to edge effects as the tapping tip is scanned across the sample. Distinct changes in surface features are evident for the undoped poly(**4c**) (Figures 7E) as compared to the previous samples. The surface is composed of small clusters packed tightly into irregular domains. There are valleys or channels between taller clusters, which range from 120 to 260 nm in depth, with a rms roughness of 71 nm. The diameter of the grains comprising the clusters measures 164 ± 66 nm. The phase image exhibits relatively consistent color throughout areas of the surface, except at a few boundary areas of the deeper grooves (Figure 7F). Changes in surface composition are not apparent for this phase frame.

A comparison of the surfaces of as-grown p-doped films is shown in Figure 8. Irregular islands are evident for poly(**4a**) (Figure 8A) ranging from 0.4 to 2.8 μm in lateral dimensions. The heights of the angular domains range from 100 to 540 nm, with an rms roughness of 91 nm which is not significantly different from that of the undoped sample. For the most part, the surface features of the undoped versus doped poly(**4a**) samples are indistinguishable. This is not really surprising because of the nonelectroactive character of this polymer in both reduced and oxidized forms, as demonstrated by cyclic voltammetry experiments. Even the phase frames exhibit markedly similar color contrast. The surface features of the doped and undoped films of poly(**4b**) are found to be slightly different at the nanoscale. Smooth round structures are apparent for doped poly(**4b**), which range from 0.1 to 1.8 μm in lateral dimensions (Figure 8C). The globular domains range from 29 to 320 nm in height, and the rms roughness is more than two times higher than that estimated for the undoped sample, namely 50 nm against 19 nm. At a local level, the round globular areas cover approximately 18% of the surface. More significant morphology changes are evident when comparing the doped and undoped poly(**4c**) films. The sizes of the nanoclusters and assembled domains have larger dimensions for the doped sample (Figure 8E). The depth of the channels between taller aggregate domains measures from 68 to 430 nm. The nanoclusters that pack tightly into surface aggregates are slightly larger and have an oval shape which is more elongated for the doped sample. As for poly(**4b**), the rms surface roughness of doped poly(**4c**) is also two times higher than that estimated for the undoped sample, namely 170 nm against ca. 70 nm. The phase image (Figure 8F) reveals more clearly the arrangement and packing of the round nanoclusters, which are more irregularly shaped and polydisperse in size. The undoped samples exhibit very small, regular shaped features, whereas the domains of the doped sample contain more random sizes and shapes for the nanoclusters. Globally, the AFM analysis of poly(**4b**) and poly(**4c**) films shows a more compact and less rough structure of insulating undoped samples compared with conducting doped samples, which is in agreement with electrochemical data of these polymers (vide supra).

Conducting Probe AFM Characterizations. For our study, the local conductive properties of the doped cobaltabisdicarbollide-functionalized films were evaluated using conductive probe AFM by measuring the current I flowing through the polymer/gold surface junction in ambient conditions, as a function of the applied voltage V. The $I-V$ profiles were generated by measuring the current as the voltage was incrementally swept from −3 to +3 V. A comparison of $I-V$ profiles plotted for the as-grown doped films is shown in Figure 9. Each curve is an average of 12 data sets acquired at different locations of the surface. The differences in the current measured for each polymer can

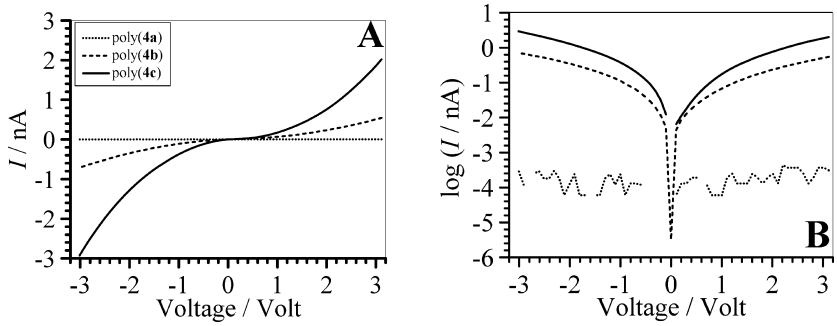

FIGURE 9. (A) Current−voltage curves and (B) corresponding semilog plots for as-grown doped poly(4a), poly(4b), and poly(4c), acquired under ambient conditions.

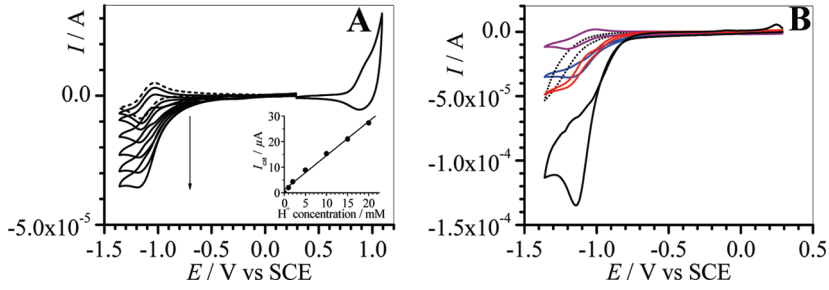

FIGURE 10. (A) Cyclic voltammograms at 0.1 V s^{-1} of a poly(4b)-coated glassy carbon (1 mm diameter) electrode in CH_3CN + 0.1 M Bu_4NPF_6 in the absence (dashed line) and in the presence of 1, 2, 5, 10, 15, and 20 mM HBF_4 (solid lines). The consumed electropolymerization charge is 64 mC cm^{-2}. (Inset) Corresponding I_{cat} vs H^+ concentration plot with I_{cat}, the electrocatalytic current (difference between the reduction currents observed in the presence and in the absence of H^+) determined at −1.15 V vs SCE. (B) Effect of the poly(4b) thickness on the electrocatalytic reduction of H^+ at 20 mM. The consumed electropolymerization charge is 25 (red), 50 (black), 64 (blue), and 255 mC cm^{-2} (purple). The dotted line corresponds to the cyclic voltammetry curve obtained at the bare glassy carbon electrode.

be confidently related to the differences in their conductivity properties because the thickness of the studied polymer films was almost similar (close to 4.0 ± 0.5 μm) and the same contact force was applied to each sample. The $I-V$ profile for poly(**4a**) exhibits no measurable current over the range of applied voltage (±3 V), which is consistent with the insulating character of this film. The profiles for poly(**4b**) and poly(**4c**) demonstrate that poly(**4c**) is more conducting than poly(**4b**), which is consistent with the more conjugated character of poly(**4c**) as determined from optical data. From corresponding semilog plots, it can be evidenced the almost symmetrical character of conduction profiles. Indeed, the rectification factors measured at ±2.0 V are 0.7 and 0.6 for poly(**4b**) and poly(**4c**), respectively. The non asymmetry of these curves suggests that poly(**4b**) and poly(**4c**) behave like heavily doped semiconductors rather than pure semiconductors for which asymmetrical current responses are usually observed (67, 68). The mean conductivity of these films was estimated using eq 2

$$\sigma = d/(A_t R) \qquad (2)$$

where σ is the electron conductivity, d is the polymer film thickness, and R is the resistance of the polymer sample, which is equal to the inverse of the slope of the $I-V$ curve. Because the $I-V$ curve is not linear, the slope was estimated from the linear fit of the curve. A_t is the area of the AFM tip in contact with the surface computed as $A_t = \pi r^2$, with $r \approx$ 35 nm, as the contact radius between tip and sample (68). An average conductivity of 1.4×10^{-4} S cm^{-1} and 7.5×10^{-4} S cm^{-1} were calculated for poly(**4b**) and poly(**4c**), respectively. Such conductivity values well-match those usually reported for other conducting metallopolymers (69–71).

3.5. Electrocatalytic Reduction of Protons at Cobaltabisdicarbollide-Functionalized Polymers. Redox-active metal centers, such as cobalt(III) bisdicarbollide, can provide efficient sites for electrocatalytic experiments at modified electrodes. As a proof-of-concept, we demonstrate that the reduction of protons to dihydrogen can be efficiently electrocatalyzed by the cobalt(II) form of the metal center incorporated in the host polythiophene matrix. As illustrated for the case of poly(**4b**), the electrochemical response of the bound Co(III)/Co(II) system is dramatically changed upon the addition of H^+ in the electrolytic medium (Figure 10A). An increase in the reduction wave of Co(III) to Co(II) is observed, the intensity of which is found to vary linearly with the proton concentration. A simple electrocatalytic mechanism consistent with our data can be written as follows.

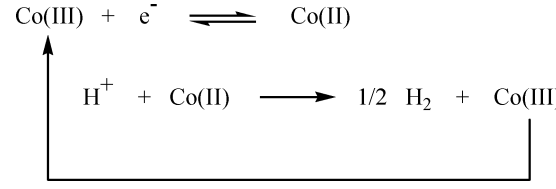

Compared with the cyclic voltammogram obtained for the direct reduction of H^+ at the bare glassy carbon electrode, the electrocatalytic effect of the immobilized metal center is evident and leads to a significant shift of the cyclic

voltammogram towards less negative potentials (Figure 10B). As commonly observed for catalysis at redox polymer coated electrodes (72), the electrocatalytic activity of cobaltabisdicarbollide-functionalized polythiophene films is strongly dependent on the film thickness. For the thinnest films, the increase in the film thickness produces the expected increase of the catalytic current as a result of an increase in the surface coverage of cobalt catalyst. The catalytic effect is maximum for a film electrogenerated with a ca. 50 mC cm^{-2} charge and decreases dramatically for thicker films. For the latter situation, the catalysis becomes kinetically controlled by the transport of charge and/or the diffusion of the substrate through the film (72), which is entirely consistent with the thickness-dependent Co(III)/Co(II) electrochemical response (vide supra).

Analysis of the data reported on Figure 10B for the optimum polymer thickness (black curve, 50 mC cm^{-2} electropolymerization charge) shows that the overpotential for hydrogen evolution is significantly decreased by ca. 230 mV with respect to that obtained with the bare glassy carbon electrode (measured for a current density of 1.4 mA cm^{-2} in the presence of 20 mM HBF_4). Despite the improved performance of the optimized modified electrode for proton reduction, the absolute potential for catalysis remains fairly negative (ca. −0.85 V vs. SCE at 1.4 mA cm^{-2}, black curve Figure 10B). We note, however, that this potential compares well with the potential range where most of the synthetic metal complexes hydrogenase mimics that have been reported so far operate (in similar organic electrolytes) (73).

4. CONCLUDING REMARKS

The electrochemical oxidation of bis(bithienyl) and bis(terthienyl) cobalt(III)bisdicarbollide complexes yielded conducting metallopolymers with quaterthienyl and sexithienyl segments, respectively. The electrochemical response of such polymers showed two reversible well-separated redox processes attributed to the Co(III)/Co(II) couple and the *p*-doping of the organic polymer backbone. Although the metal-based process was totally reversible for thin films, a decrease in the rate of electron hopping between the metal centers was observed upon increasing the film thickness. This was consistent with an electron transfer controlled by the diffusion of electrolyte countercations through the film to ensure the electroneutrality. Moreover, the optical data indicated a weak electronic communication between the oligothienyl segments through the cobaltabisdicarbollide bridge. However, the presence of the metallic complex accounted for the lowly doped character of the polymer film and the measured conductivity values below 1×10^{-3} S cm^{-1}, which are much lower than those commonly found for doped polythiophene films. The electrocatalytic results suggest that conducting polymers containing in chain metallabisdicarbollide could find interesting applications as robust and efficient catalysts for the activation of small molecules, and especially for the important H^+/H_2 interconversion (74). So far, little attention has been paid to the catalytic potential of metallabisdicarbollides, as most catalysis studies have involved the metal dicarbollide fragment as a substitute/alternative to a piano-stool metallocene framework (75). We believe that the present work opens the way for refining this promising new type of electrocatalytic material in terms of the nature of the conducting polymer, length of monomer, nature of the metal, and thickness of polymer. Toward the challenging goal of preparing highly conducting carborane-based metallopolymers with versatile electrocatalytic properties, other electropolymerizable metallabisdicarbollides with metal cations, such as Fe, Ni, and Cu, will be investigated in order to obtain different overlaps of the electrochemical responses for the metal and the polymer backbone.

Acknowledgment. We thank the CINES (Montpellier) for allocation of computing time. J.C.G. acknowledges support from the National Science Foundation (DMR-0906873).

Supporting Information Available: High-resolution ESI mass spectra of **4a**, **4b**, and **4c**; UV−vis spectra of **4a**, **4b**, and **4c** (PDF). This material is available free of charge via the Internet at http://pubs.acs.org.

REFERENCES AND NOTES

(1) Reed, C. A. *Acc. Chem. Res.* **1998**, *31*, 133–139.
(2) Plesek, J. *Chem. Rev.* **1992**, *92*, 269–278, and references therein.
(3) Hawthorne, M. F.; Young, D. C.; Andrews, T. D.; Howe, D. V.; Pilling, R. L.; Pitts, A. D.; Reintjes, M.; Warren, L. F., Jr.; Wegner, P. A. *J. Am. Chem. Soc.* **1968**, *90*, 879–896.
(4) Hawthorne, M. F.; Young, D. C.; Wegner, P. A. *J. Am. Chem. Soc.* **1970**, *87*, 1818–1819.
(5) Grüner, B.; Plesek, J.; Baca, J.; Cisarova, I.; Dozol, J. F.; Rouquette, H.; Vinas, C.; Selucky, P.; Rais, J. *New J. Chem.* **2002**, *26*, 1519–1527.
(6) Stoica, A.-I.; Vinas, C.; Teixidor, F. *Chem. Commun.* **2009**, *33*, 4988–4990.
(7) Rojo, I.; Teixidor, F.; Vinas, C.; Kivekaes, R.; Sillanpaeae, R. *Chem.—Eur. J.* **2004**, *10*, 5376–5385.
(8) Hao, E.; Zhang, M. E. W.; Kadish, K. M.; Fronczek, F. R.; Courtney, B. H.; Vicente, M. G. H. *Bioconjugate Chem.* **2008**, *19*, 2171–2181.
(9) Hao, E.; Jensen, T. J.; Courtney, B. H.; Vicente, M. G. H. *Bioconjugate Chem.* **2005**, *16*, 1495–1502.
(10) Hawthorne, M. F.; Zink, J. I.; Skelton, J. M.; Bayer, M. J.; Liu, C.; Livshits, E.; Baer, R.; Neuhauser, D. *Science* **2004**, *303*, 1849–1851.
(11) Hawthorne, M. F.; Ramachandran, B. M.; Kennedy, R. D.; Knobler, C. B. *Pure Appl. Chem.* **2006**, *78*, 1299–1304.
(12) Soloway, A. H.; Tjarks, W.; Barnum, B. A.; Rong, F.-G.; Barth, R. F.; Codogni, I. M.; Wilson, J. G. *Chem. Rev.* **1998**, *98*, 1515–1562.
(13) Hawthorne, M. F.; Maderna, A. *Chem. Rev.* **1999**, *99*, 3421–3434.
(14) Barth, R. F.; Coderre, J. A.; Vicente, M. G. H.; Blue, T. E. *Clin. Cancer Res.* **2005**, *11*, 3987–4002.
(15) Kaszynski, P.; Douglass, A. G. *J. Organomet. Chem.* **1999**, *581*, 28–38.
(16) Kottas, G. S.; Clarke, L. I.; Horinek, D.; Michl, J. *Chem. Rev.* **2005**, *105*, 1281–1376.
(17) Kabachii, Y. A.; Valetskii, P. M. *Int. J. Polym. Mater* **1990**, *14*, 263–273.
(18) Schöberl, U.; Magnera, T. F.; Harrison, R. M.; Fleischer, F.; Pflug, J. L.; Schwab, P. F. H.; Meng, X.; Lipiak, D.; Noll, B. C.; Allured, V. S.; Rudalevige, T.; Lee, S.; Michl, J. *J. Am. Chem. Soc.* **1997**, *119*, 3907–3917.
(19) Colquhoun, H. M.; Herbertson, P. L.; Wade, K.; Baxter, I.; Williams, D. J. *Macromolecules* **1998**, *31*, 1694–1696.
(20) Fox, M. A.; Wade, K. *J. Mater. Chem.* **2002**, *12*, 1301–1306.
(21) Kimura, H.; Okita, K.; Ichitani, M.; Sugimoto, T.; Kuroki, S.; Ando, I. *Chem. Mater.* **2003**, *15*, 355–362.
(22) Bekasova, N. I. *Russ. Chem. Rev.* **1984**, *53*, 61–76.
(23) David, V.; Vinas, C.; Teixidor, F. *Polymer* **2006**, *47*, 4694–4702.
(24) Masalles, C.; Borros, S.; Vinas, C.; Teixidor, F. *Adv. Mater.* **2000**, *12*, 1199–1202.

(25) Masalles, C.; Llop, J.; Vinas, C.; Teixidor, F. *Adv. Mater.* **2002**, *14*, 826–829.
(26) Masalles, C.; Teixidor, F.; Borros, S.; Vinas, C. *J. Organomet. Chem.* **2002**, *657*, 239–246.
(27) Hao, E.; Fabre, B.; Fronczek, F. R.; Vicente, M. G. H. *Chem. Mater.* **2007**, *19*, 6195–6205.
(28) Hao, E.; Fabre, B.; Fronczek, F. R.; Vicente, M. G. H. *Chem. Commun.* **2007**, 4387–4389.
(29) Fabre, B.; Clark, J. C.; Vicente, M. G. H. *Macromolecules* **2006**, *39*, 112–119.
(30) Fabre, B.; Chayer, S.; Vicente, M. G. H. *Electrochem. Commun.* **2003**, *5*, 431–434.
(31) Barrière, F.; Fabre, B.; Hao, E.; LeJeune, Z. M.; Hwang, E.; Garno, J. C.; Nesterov, E. E.; Vicente, M. G. H. *Macromolecules* **2009**, *42*, 2981–2987.
(32) Peterson, J. J.; Simon, Y. C.; Coughlin, E. B.; Carter, K. R. *Chem. Commun.* **2009**, 4950–4952.
(33) Kokado, K.; Tokoro, Y.; Chujo, Y. *Macromolecules* **2009**, *42*, 2925–2930.
(34) Holliday, B. J.; Swager, T. M. *Chem. Commun.* **2005**, 25–36.
(35) Hohenberg, P.; Kohn, W. *Phys. Rev.* **1964**, *136*, B864–B871.
(36) Parr, R. G.; Yang, W. *Density-Functional Theory of Atoms and Molecules*; Oxford University Press: Oxford, U.K., 1989.
(37) Becke, A. D. *Phys. Rev.* **1988**, *38*, 3098–3100.
(38) Becke, A. D. *J. Chem. Phys.* **1993**, *98*, 1372–1377.
(39) Becke, A. D. *J. Chem. Phys.* **1993**, *98*, 5648–5652.
(40) Lee, C.; Yang, W.; Parr, R. G. *Phys. Rev. B* **1988**, *37*, 785–789.
(41) Frisch, M. J.; Trucks, G. W.; Schlegel, H. B.; Scuseria, G. E.; Robb, M. A.; Cheeseman, J. R.; Montgomery, J., J. A.; Vreven, T.; Kudin, K. N.; Burant, J. C.; Millam, J. M.; Iyengar, S. S.; Tomasi, J.; Barone, V.; Mennucci, B.; Cossi, M.; Scalmani, G.; Rega, N.; Petersson, G. A.; Nakatsuji, H.; Hada, M.; Ehara, M.; Toyota, K.; Fukuda, R.; Hasegawa, J.; Ishida, M.; Nakajima, T.; Honda, Y.; Kitao, O.; Nakai, H.; Klene, M.; Li, X.; Knox, J. E.; Hratchian, H. P.; Cross, J. B.; Adamo, C.; Jaramillo, J.; Gomperts, R.; Stratmann, R. E.; Yazyev, O.; Austin, A. J.; Cammi, R.; Pomelli, C.; Ochterski, J. W.; Ayala, P. Y.; Morokuma, K.; Voth, G. A.; Salvador, P.; Dannenberg, J. J.; Zakrzewski, V. G.; Dapprich, S.; Daniels, A. D.; Strain, M. C.; Farkas, O.; Malick, D. K.; Rabuck, A. D.; Raghavachari, K.; Foresman, J. B.; Ortiz, J. V.; Cui, Q.; Baboul, A. G.; Clifford, S.; Cioslowski, J.; Stefanov, B. B.; Liu, G.; Liashenko, A.; Piskorz, P.; Komaromi, I.; Martin, R. L.; Fox, D. J.; Keith, T.; Al-Laham, M. A.; Peng, C. Y.; Nanayakkara, A.; Challacombe, M.; Gill, P. M. W.; Johnson, B.; Chen, W.; Wong, M. W.; Gonzalez, C.; Pople, J. A. *Gaussian 03, Revision D.02*; Gaussian, Inc.: Pittsburgh, PA, 2003.
(42) Hay, P. J.; Wadt, W. R. *J. Chem. Phys.* **1985**, *82*, 270–283.
(43) Wadt, W. R.; Hay, P. J. *J. Chem. Phys.* **1985**, *82*, 284–298.
(44) Hay, P. J.; Wadt, W. R. *J. Chem. Phys.* **1985**, *82*, 299–310.
(45) Flükiger P., Lüthi H. P., Portmann S., Weber J. *MOLEKEL 4.3*; Swiss Center for Scientific Computing: Manno, Switzerland, 2000.
(46) Wilcox, D.; Dove, B.; McDavid, D.; Greer, D. *UTHSCSA Image Tool for Windows version 3.00*; The University of Texas Health Science Center: San Antonio, TX, 1995—2002.
(47) Zhu, Y.; Millet, D. B.; Wolf, M. O.; Rettig, S. J. *Organometallics* **1999**, *18*, 1930–1938.
(48) Jiang, W.; Knobler, C. B.; Hawthorne, M. F. *Inorg. Chem.* **1996**, *35*, 3056–3058.
(49) Fox, M. H.; Gill, W. R.; Herbertson, P. L.; MacBride, J. A. H.; Wade, K.; Colquhoun, H. M. *Polyhedron* **1996**, *15*, 565–571.
(50) Endo, Y.; Songkram, C.; Yamasaki, R.; Tanatani, A.; Kagechika, H.; Takaishi, K.; Yamaguchi, K. *J. Organomet. Chem.* **2002**, *657*, 48–58.
(51) Rudakov, D. A.; Shirokii, V. L.; Knizhnikov, V. A.; Bazhanov, A. V.; Vecher, E. I.; Maier, N. A.; Potkin, V. I.; Ryabtsev, A. N.; Petrovskii, P. V.; Sivaev, I. B.; Bregadze, V. I.; Eremenko, I. L. *Russ. Chem. Bull.* **2004**, *53*, 2554–2557.
(52) Kennedy, R. D.; Knobler, C. B.; Hawthorne, M. F. *Inorg. Chem.* **2009**, *48*, 9377–9384.
(53) Nuñez, R.; Tutusaus, O.; Teixidor, F.; Viñas, C.; Sillanpää, R.; Kivekäs, R. *Chem.—Eur. J.* **2005**, *11*, 5637–5647.
(54) Zhu, Y.; Wolf, M. O. *Chem. Mater.* **1999**, *11*, 2995–3001.
(55) Higgins, S. J.; Jones, C. L.; Francis, S. M. *Synth. Met.* **1999**, *98*, 211–214.
(56) Bard, A. J.; Faulkner, L. R. In *Electrochemical Methods. Fundamentals and Applications*; Wiley & Sons: New York, 1980.
(57) δ is calculated from the integration of the cyclic voltammetry curve corresponding to the oxidation step of the polymer matrix, assuming an electropolymerization yield of 100%.
(58) Kingsborough, R. P.; Swager, T. M. *Adv. Mater.* **1998**, *10*, 1100–1104.
(59) Audebert, P.; Capdevielle, P.; Maumy, M. *New J. Chem.* **1992**, *16*, 697–703.
(60) Matel, L.; Macasek, F.; Rajec, P.; Hermanek, S.; Plesek, J. *Polyhedron* **1982**, *1*, 511–519.
(61) Rojo, I.; Teixidor, F.; Vinas, C.; Kivekäs, R.; Sillanpää, R. *Chem.—Eur. J.* **2003**, *9*, 4311–4323.
(62) Zotti, G.; Schiavon, G. *Synth. Met.* **1990**, *39*, 183–190.
(63) Fichou, D.; Horowitz, G.; Garnier, F. *Synth. Met.* **1990**, *39*, 125–131.
(64) Havinga, E. E.; Rotte, I.; Meijer, E. W.; Hoeve, W. T.; Wynberg, H. *Synth. Met.* **1991**, *41*, 473–478.
(65) Chosrovian, H.; Rentsch, S.; Grebner, D.; Dahm, D. U.; Birckner, E.; Naarmann, H. *Synth. Met.* **1993**, *60*, 23–26.
(66) Wallace, G. G.; Spinks, G. M.; Kane-Maguire, L. A. P.; Teasdale, P. R. In *Conductive Electroactive Polymers*, 2nd ed.; CRC Press: Boca Baton, FL, 2003.
(67) Lee, H. J.; Park, S.-M. *J. Phys. Chem. B* **2004**, *108*, 1590–1595.
(68) Wu, C.-G.; Chang, S.-S. *J. Phys. Chem. B* **2005**, *109*, 825–832.
(69) Hjelm, J.; Handel, R. W.; Hagfeldt, A.; Constable, E. C.; Housecroft, C. E.; Forster, R. J. *J. Phys. Chem. B* **2003**, *107*, 10431–10439.
(70) Nishihara, H.; Kurashina, M.; Murata, M. *Macromol. Symp.* **2003**, *196*, 27–38.
(71) Vidal, P.-L.; Divisia-Blohorn, B.; Bidan, G.; Hazemann, J.-L.; Kern, J.-M.; Sauvage, J.-P. *Chem.—Eur. J.* **2000**, *6*, 1663–1673.
(72) Andrieux, C. P.; Savéant, J.-M. In *Molecular Design of Electrode Surfaces*; Murray, R. W., Ed.; Wiley & Sons: New York, 1992; Vol. XXII, pp 207—270.
(73) Tard, C.; Pickett, C. J. *Chem. Rev.* **2009**, *109*, 2245–2274.
(74) Le Goff, A.; Artero, V.; Jousselme, B.; Tran, P. D.; Guillet, N.; Métayé, R.; Fihri, A.; Palacin, S.; Fontecave, M. *Science* **2009**, *326*, 1384–1387.
(75) Tutusaus, O.; Viñas, C.; Núñez, R.; Teixidor, F.; Demonceau, A.; Delfosse, S.; Noels, A. F.; Mata, I.; Molins, E. *J. Am. Chem. Soc.* **2003**, *125*, 11830–11831.

AM9007424